Gravity–Mode Instabilities in Models of Post–Extreme Horizontal Branch Stars: Another Class of Pulsating Stars?

S. Charpinet, G. Fontaine, and P. Brassard

Département de Physique, Université de Montréal, C.P. 6128, Succ. Centre-Ville,

Montréal, Québec, Canada, H3C 3J7

charpinet, fontaine, brassard@astro.umontreal.ca

and

Ben Dorman[1]

Laboratory for Astronomy and Solar Physics, NASA/GSFC, Greenbelt, MD 20771

Ben.Dorman@gsfc.nasa.gov

Received _____; accepted _____

Submitted to *The Astrophysical Journal (Letters)*

[1]Also, Department of Astronomy, University of Virginia, P.O. Box 3818, Charlottesville, VA 22903–0818

ABSTRACT

We present new results of a stability analysis of realistic models of post–extreme horizontal branch stars. We find that g–mode instabilities develop in some of these models as a result of a potent ϵ–mechanism associated with the presence of an active H–burning shell. The ϵ–process drives low order and low degree g–modes with typical periods in the range 40–125 s. The unstable models populate a broad instability strip covering the interval 76,000 K $\gtrsim$ $T_{\rm eff}$ $\gtrsim$ 44,000 K, and are identified with low–mass DAO white dwarfs. They descend from stars that reach the zero–age "extended" horizontal branch with H–rich envelope masses $M_{\rm env}$ $\gtrsim$ 0.0010 $M_{\odot}$. Our computations indicate that some DAO stars should show luminosity variations resulting from pulsational instabilities. We suggest looking for brightness variations in six particularly promising candidates.

Subject headings: stars: interiors−stars: oscillations−subdwarfs−white dwarfs

1. ASTROPHYSICAL CONTEXT

We have recently embarked in a systematic investigation of the asteroseismological potential of stellar models on the extreme horizontal branch (EHB) and beyond. This was made possible thanks to significant progress in our ability to compute increasingly sophisticated and realistic models for this relatively neglected phase of stellar evolution (see, e.g., Dorman 1995 for a review). The models of interest are low–mass objects ($M \lesssim 0.5\ M_{\odot}$) with outer H–rich envelopes too thin to reach the AGB after core helium exhaustion. Such models cannot sustain significant H–shell burning during core helium burning evolution. The core He burning phase, of typical length $\sim 10^8$ yr, is identified with subdwarf B (sdB) stars. The stars have atmospheric parameters found in the ranges 40,000 K $\gtrsim T_{\rm eff} \gtrsim$ 24,000 K and $6.2 \gtrsim \log g \gtrsim 5.1$ (see Saffer et al. 1994 and references therein).

A stability analysis of stellar models in the sdB phase of evolution has led us to the discovery of an efficient driving mechanism due to an opacity bump associated with iron ionization (Charpinet et al. 1996). It was found that both radial and nonradial (p, f, and g) low order modes could be excited in some of these models. On this basis, we made the prediction that a subclass of sdB stars should show luminosity variations resulting from pulsational instabilities. The independent and exciting discoveries of the first real pulsating sdB stars in South Africa (Kilkenny et al. 1997; Koen et al. 1997; Stobie et al. 1997; O'Donoghue et al. 1997) gave us confidence in the basic validity of our models. They also led to further developments on the observational front (Billères et al. 1997) and to refinements of the physical description of our iron bump mechanism (Charpinet et al. 1997).

While the observational and theoretical foundations for the pulsating sdB stars now appear to be well established, the asteroseismological potential of their descendants, the post–EHB stars, has not been investigated and remains of great interest. During the post–core–exhaustion phase the stars contract and the H–burning shell finally "turns on".

With insufficient hydrogen energy to force a red–giant star envelope, the stars live in the so–called "AGB–Manqué" phase (Greggio & Renzini 1990) for a period similar to the equivalent Early (i.e., pre–Thermal Pulsing) AGB evolution phase, $2 - 4 \times 10^7$ yr. These post–EHB, He–shell–burning models are associated with the field subdwarf O stars (Dorman, O'Connell, & Rood 1995 and references therein). A majority of these stars cluster around $T_{\rm eff} \sim 45{,}000$ K and $\log g \sim 5.5$ (Dreizler 1993). Ultimately, the models join the white dwarf cooling tracks near $T_{\rm eff} \sim 80{,}000$ K and are identified, in the early white dwarf phase, to the low–gravity DAO white dwarfs (Bergeron et al. 1994).

¿From an asteroseismological standpoint, the ignition of hydrogen at the base of the H–rich outer layer in these hot, post–EHB models is particularly interesting. Up to 50% of the luminosity of the star may be provided by hydrogen burning in a thin shell in these evolved models. The location of the H–burning shell strongly suggests that a potent ϵ–mechanism might drive pulsation modes there (see below). In contrast, the He–burning shell appears to be located too deep at the outset to play a key role in destabilizing modes. Moreover, we do not expect the iron bump mechanism uncovered in sdB models to be relevant to post–EHB models as they are too hot (see Charpinet et al. 1997).

In this Letter, we report on the salient features of a stability analysis we carried out for realistic models of post–EHB stars, and on our discovery of pulsational instabilities in some of them.

2. STABILITY ANALYSIS OF POST–EHB MODELS

The equilibrium models employed in this investigation are full stellar models taken from seven distinct evolutionary sequences. The sequences span the evolution from the zero–age–EHB (ZAEHB) to the cool white dwarf phase. The evolutionary models were

computed with the methods described in Dorman (1992a,b) and Dorman et al. (1993), but included improvements in the constitutive physics. The new models use the OPAL opacities described by Rogers & Iglesias (1992) computed in December 1993, which adopted the element mix referred to as "Grevesse & Noels 1993." Where necessary (during He–flashes), we used new low temperature opacities by D. R. Alexander (1995, private communication, described in Alexander & Ferguson 1994) which were computed with the same element mix. These smoothly match the OPAL opacity set within the hydrogen ionization zone. The other difference in the input physics was the use of the Itoh et al. (1983; 1993a,b; 1994a,b) conductive opacities.

Five of the sequences (the same as those considered by Charpinet et al. 1996) correspond to the evolution of an AGB–Manqué star with a core mass of 0.4758 $M_{\odot}$. The sequences differ in that different initial envelope masses on the ZAEHB are considered: $M_{\rm env}$ = 0.0002, 0.0012, 0.0022, 0.0032, and 0.0042 $M_{\odot}$. Two additional sequences with core masses of 0.4690 $M_{\odot}$ and ZAEHB envelope masses of 0.0001 and 0.0007 $M_{\odot}$ have been added in the meantime to provide a better mapping of the sdB region in the $T_{\rm eff}$–log g diagram. In all cases, the composition of the envelopes was assumed to be solar (X = 0.70388, Z = 0.01718), derived from calibrating a solar model sequence to $\log L/L_{\odot} = 0$, $T_{\rm eff}$ = 5770 K at age 4.6 Gyr.

Figure 1 illustrates the evolutionary tracks for three of our sequences in the $T_{\rm eff}$–log g plane. For comparison purposes, the positions of 213 known sdB stars (according to R.A. Saffer, private communication) are shown in the upper right region of the diagram, while the positions of the DAO and hot DA white dwarfs analyzed by Bergeron et al. (1994) are shown in the lower part of the figure. Of prime interest in the present context, is the conclusion of Bergeron et al. (1994) that six of the DAO stars in their sample (those distributed about our evolutionary tracks) are post–EHB objects. In contrast, the

majority of the hot white dwarfs they discuss have higher gravities (see Fig. 1), and must be considered as post–AGB stars (see Bergeron et al. 1994).

In the present effort, we have carried out a stability analysis for all of our post–EHB models, i.e., those beyond the sdB phase itself. Those models are characterized by double He– and H–shell burning. We considered all modes with $l = 0$, 1, 2, and 3 in the 5–500 s period window. This was done with the finite–element nonadiabatic pulsation code briefly described in Fontaine et al. (1994) and in Brassard, Fontaine, & Bergeron (1997). We found that, in four of our sequences, the ϵ–mechanism produced by the H–burning shell is sufficiently potent to drive low order g–modes in models located at the beginning of the white dwarf branch of the evolutionary tracks. The unstable models define a broad strip covering the range 76,000 K $\gtrsim$ $T_{\rm eff}$ $\gtrsim$ 44,000 K and are identified with the DAO phase of post–EHB evolution. The thick line segments along two evolutionary tracks in Figure 1 show a mapping of the instability strip. The sequences with the smaller H–rich envelope masses on the ZAEHB (i.e., those with $M_{\rm env} = 0.0001$, 0.0002, and 0.0007 $M_\odot$) have less active H–burning shells throughout the evolution. While the ϵ–mechanism due to such shells still produces significant local driving, particularly within the instability strip, it is not strong enough to overcome radiative damping processes in these models.

A typical unstable model is model #32 belonging to the sequence with $M_{\rm core} = 0.4758$ $M_\odot$and $M_{\rm env} = 0.0012$ $M_\odot$, whose evolutionary track is illustrated in Fig. 1. It has an age of 1.39×10^8 yr (time elapsed since the ZAEHB), a surface gravity $\log g = 7.24$, a luminosity $L = 6.31$ $L_\odot$, and an effective temperature $T_{\rm eff} = 55{,}560$ K. Table 1 gives the periods and the e–folding times (for the unstable modes) of the lowest order pulsation modes for this model. The radial modes ($l = 0$) are all stable and not listed in the table. In this, and in all other models showing instabilities, only the g–modes are excited; the p–modes are never driven. The table indicates that the lowest order g–modes ($k = 1$, 2, and/or 3) are excited

and span a period range 42–123 s. The e–folding times must be compared with the time it takes for a post–EHB star to cross the instability strip. Since this time is approximately equal to 4.0×10^6 yr, substantially longer than most of the e–folding times, it would appear that the excited pulsations have plenty of time to develop observable amplitudes.

Figure 2 illustrates some structural properties for our representative model. The upper panel indicates, among other things, the location of the He– and H–burning shells as well as the magnitude of the nuclear energy generation rate there (dotted curve). On the scale used here, the contribution of the He–burning shell is insignificant. The lower panel shows the compositional stratification as well as the luminosity profile. The latter demonstrates that about 40% of the total luminosity of the model is due to H–shell burning at the base of the H–rich envelope. At the epoch of the model, some 68% of the hydrogen in the original ZAEHB envelope of 0.0012 $M_\odot$ has been consumed. Explicit tests carried out by switching off ϵ_H and/or ϵ_{He} in the pulsation calculations demonstrate, as implied by the upper panel of Figure 2, that all the driving is caused by the ϵ–mechanism generated by the H–burning shell.

3. DISCUSSION

The g–mode instabilities uncovered here are very similar in nature to the pulsational instabilities discussed by Kawaler (1988; see also Sienkiewicz 1980) in the context of the much more luminous and hotter central stars of planetary nebulae. Standard models of these post–AGB stars also show a double–shell burning structure. As in Kawaler (1988), the ϵ–process provides here both the driving force and a filter mechanism (selecting only a few modes as unstable), but, unlike the case for those very luminous models, only the H–burning shell contributes to the process in the present situation.

The g–modes are favored for instability because, in the course of post–EHB evolution, their region of formation migrates from the core in the sdB phase (Charpinet et al. 1996, 1997) to the outer envelope in the cool pulsating white dwarfs of the ZZ Ceti type (see, e.g., Brassard et al. 1992). In the post–EHB DAO phase, g–modes are mostly sensitive to the physical conditions in the deep envelope, where the H–burning shell is located. In contrast, the He–burning shell is rather located in the core (see Fig. 2, upper panel), is less active, and thus plays no significant role.

The g–modes that are driven are those with oscillation amplitudes that are large in the H–shell–burning region. In practice, this means that the largest maximum in the temperature perturbation of a mode (usually the maximum located nearest to the surface) should nearly coincide with the H–burning shell. As the radial index k of a mode increases, this maximum in the temperature perturbation moves outward, ultimately reaching a location beyond the shell. Those modes can no longer be efficiently driven. This then provides a filter, a cutoff in k, beyond which the g–modes are stable.

In the upper panel of Figure 2, we have plotted the absolute value of the Lagrangian temperature perturbation of three modes as a function of depth in our representative model. Note that this function is normalized for each mode, so the only information of interest here is related to the relative strengths and locations of maxima for a *given* mode. The three modes illustrated belong to the sequence with $l = 1$. The mode with $k = 2$ has a period of 109.78 s and is unstable (see Table 1). The behavior of its temperature perturbation (solid curve) illustrates what was written in the previous paragraph, namely that its largest maximum nearly overlaps with the H–burning shell. This maximizes the efficiency of ϵ–driving for that mode.

The modes with $k \geq 4$ (and $l = 1$) are all stable in our representative model. The dot–dashed curve in the upper panel of Figure 2 shows that the largest maximum in the

temperature perturbation of the $k = 5$ mode (a stable mode with a period of 187.84 s; see Table 1) is located well above the shell burning region, near log q $\simeq$ –5.8, where radiative damping is important. In this specific case, the temperature perturbation also shows a node just below the H–burning shell, so the conditions are particularly unfavorable for efficient ϵ–driving for this mode. Finally, we illustrate also the behavior of the normalized temperature perturbation for a mode with $k = 8$ (not listed in Table 1, but stable and with a period of 272.70 s). Here a secondary maximum is located right in the middle of the H–burning shell, but the ensuing driving is overcome by damping in the regions above where the relative amplitude of the temperature perturbation becomes much larger.

4. CONCLUSION

The results presented in this paper strongly suggest that non–radial pulsations may be present in post–EHB evolution, and thus the methods of asteroseismology may shed light on the structure of stars in this phase. We have found that g–mode instabilities develop in realistic models of post–EHB stars. The unstable models are the descendants of stars with relatively massive ($M_{\rm env} \gtrsim 0.0010\ M_{\odot}$) H–rich envelopes on the ZAEHB, and pulsate because of the presence of an active H–burning shell at the base of the envelope. They define a broad instability strip covering the range 76,000 K $\gtrsim T_{\rm eff} \gtrsim$ 44,000 K, and are identified with low–mass DAO white dwarfs. Low order and low degree g–modes with typical periods around $\sim$ 80 s are predicted to be unstable in that instability strip.

Specifically, we suggest looking for luminosity variations in those DAO objects already identified by Bergeron et al. (1994) as post–EHB stars. Those are HZ 34, GD 651, Ton 353, PG 0834+501, Feige 55, and PG 0134+181. Of course, there is no a priori guarantee that those stars have ZAHB progenitors with envelopes in the correct mass range, since the region of temperature/gravity space occupied by the models with instabilities must be quite

thin. Also, weak mass loss (often invoked to explain the abundance anomalies of sdB stars) may succeed in thinning that envelope to the point, perhaps, of reducing significantly the ϵ–driving. In any case, the proposed observations would provide interesting constraints on the amount of hydrogen left over in these DAO stars.

This work was supported in part by the NSREC of Canada and by the fund FCAR (Québec). B.D. acknowledges support from NASA grants NAG5-700 and NAGW-4106.

Table 1. Pulsation Periods and E-folding Times for a Representative DAO Model

k	$l = 1$		$l = 2$		$l = 3$	
	P (s)	τ_e (yrs)	P (s)	τ_e (yrs)	P (s)	τ_e (yrs)
3	10.99	stable	10.48	stable	9.78	stable
2	13.63	stable	11.90	stable	11.24	stable
1	15.61	stable	15.19	stable	14.75	stable
0	$\cdots$	$\cdots$	20.70	stable	17.18	stable
1	82.37	6.99×10^6	54.11	9.98×10^5	42.41	2.42×10^5
2	109.78	9.01×10^4	69.33	1.34×10^4	50.25	1.14×10^4
3	122.73	1.14×10^4	74.59	4.70×10^4	59.59	stable
4	158.70	stable	101.64	stable	76.55	stable
5	187.84	stable	114.16	stable	87.22	stable

REFERENCES

Alexander, D. A. & Ferguson, J. W. 1994, ApJ, 437, 879

Bergeron, P., Wesemael, F., Beauchamp, A., Wood, M.A., Lamontagne, R., Fontaine, G., & Liebert, J. 1994, ApJ, 432, 305

Billères, M., Fontaine, G., Brassard, P., Charpinet, S., Liebert, J., Saffer, R.A., & Vauclair, G. 1997, ApJ, in press

Brassard, P., Fontaine, G., & Bergeron, P. 1997, in preparation

Brassard, P., Fontaine, G., Wesemael, F., & Tassoul, M. 1992, ApJS, 81, 747

Charpinet, S., Fontaine, G., Brassard, P., & Dorman, B. 1996, ApJ, 471, L103

Charpinet, S., Fontaine, G., Brassard, P., Chayer, P., Rogers, F.J., Iglesias, C.A., & Dorman, B. 1997, ApJ, in press

Dorman, B. 1992a, ApJS, 80, 701

Dorman, B. 1992b, ApJS, 81, 221

Dorman, B. 1995, in Proc. 32nd Liège Astrophysical Colloq., Stellar Evolution: What Should Be Done, ed. A. Noels, D. Fraipont-Caro, N. Grevesse, & P. Demarque (Liège: Institut d'Astrophysique), 291

Dorman, B., O'Connell, R.W., & Rood, R.T., 1995, ApJ, 442, 105

Dorman, B., Rood, R.T., & O'Connell, R.W. 1993, ApJ, 415, 596

Dreizler, S. 1993, in White Dwarfs: Advances in Observation and Theory, ed. M.A. Barstow, NATO ASI Series, 403, 287

Fontaine, G., Brassard, P., Wesemael, F., & Tassoul, M. 1994, ApJ, 428, L61

Greggio, L. & Renzini, A., 1990 ApJ, 364, 35

Itoh, N., Hayashi, H., & Kohyama, Y. 1993a, ApJ, 418, 405

Itoh, N., Hayashi, H., & Kohyama, Y. 1994a, ApJ, 436, 418

Itoh, N., Kohyama, Y. Matsumoto, N., & Seki, M. 1993b, ApJ, 404, 418

Itoh, N. & Kohyama, Y. 1994b, ApJ, 420, 943

Itoh, N., Mitake, S., Iyetomi, H., & Ichimaru, S., 1983, 273, 774

Kawaler, S.D. 1988, ApJ, 334, 220

Kilkenny, D., Koen, C., O'Donoghue, D., & Stobie, R.S. 1997b, MNRAS, 285, 640

Koen, C., Kilkenny, D., O'Donoghue, D., Van Wyk, F., and Stobie, R.S. 1997, MNRAS, 285, 645

O'Donoghue, D., Lynas-Gray, A.E., Kilkenny, D., Stobie, R.S., & Koen, C. 1997b, MNRAS, 285, 657

Rogers, F.J., & Iglesias, C.A. 1992, ApJ, 401, 361

Saffer, R.A., Bergeron, P., Koester, D., & Liebert, J. 1994, ApJ, 432, 351

Sienkiewicz, R. 1980, A&A, 85, 295

Stobie, R.S., Kawaler, S.D., Kilkenny, D., O'Donoghue, D., & Koen, C. 1997, MNRAS, 285, 651

FIGURE CAPTIONS

Fig. 1 — Typical evolutionary tracks for EHB and post–EHB models in the $T_{\rm eff}$–log g diagram. Three tracks are illustrated, each corresponding to the same initial core mass, 0.4758 $M_{\odot}$, but with ZAEHB H–rich envelope masses of 0.0042, 0.0012, and 0.0002 $M_{\odot}$. The individual models along a track are represented by small crosses, and are joined together by dotted straight line segments. They cover the evolution from the ZAEHB to the white dwarf phase. Superimposed, in the upper right corner, are the positions of 213 real sdB stars (small dots). Likewise, the positions of the known DAO (filled circles) and hot DA (open circles) white dwarfs are illustrated in the lower part of the diagram. The thick segments along two of the tracks in the DAO region correspond to the positions of unstable models driven by the ϵ–mechanism in the H–burning shell.

Fig. 2 — Lower panel: the solid curve gives the luminosity profile as a function of fractional mass depth (log q = log $(1 - M(r)/M_*)$) in our representative model. The other curves show the composition stratification. Upper panel: the dotted curve shows the magnitude of the nuclear energy generation rate in, and the location of, the He– and H–burning shell. The other curves refer to the amplitude of the relative Lagrangian perturbation of the temperature for three g–mode overtones with $l = 1$. Only the mode with $k = 2$ is excited.

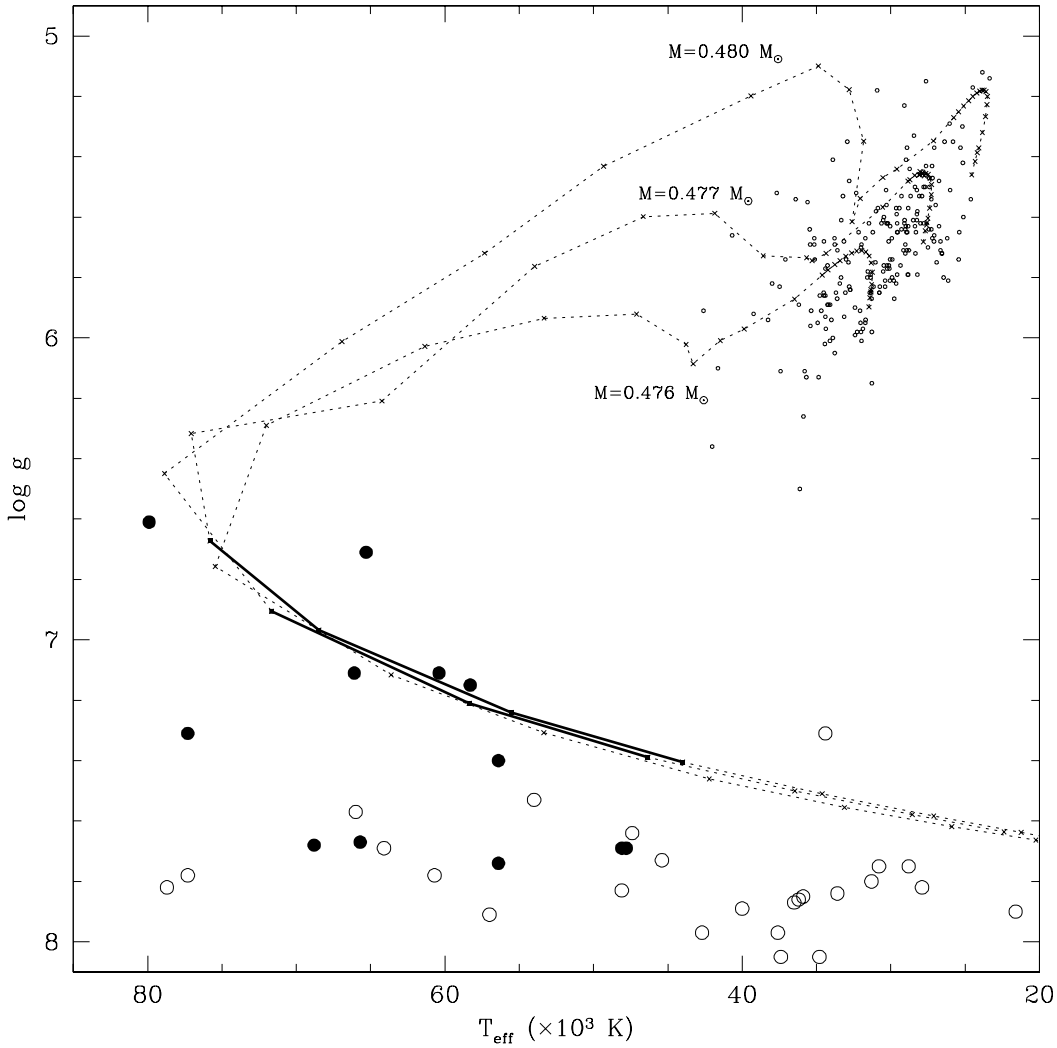

Figure 1

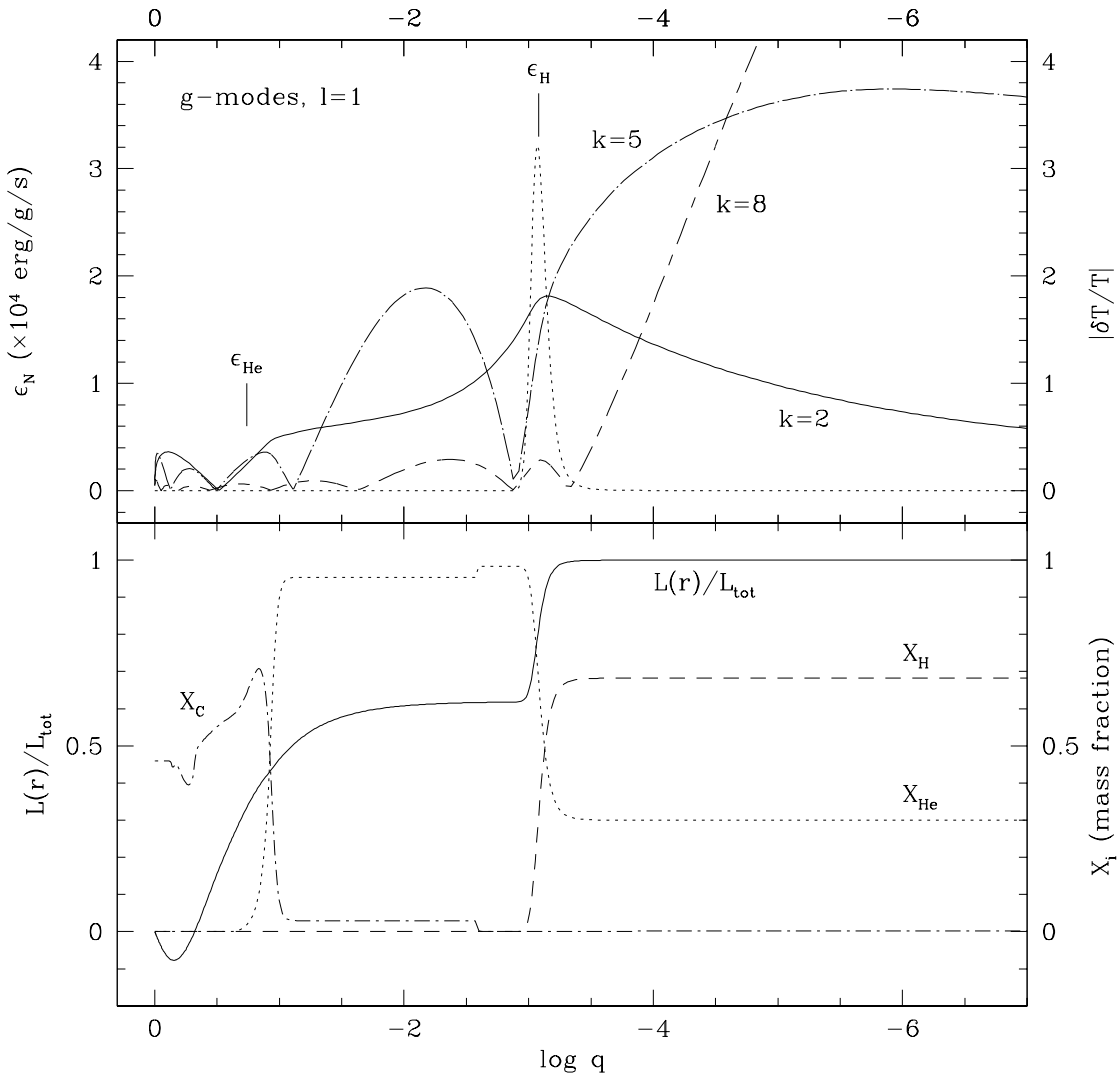
g−modes, l=1
ϵ_H
ϵ_{He}
k=5
k=8
k=2
ϵ_N ($\times 10^4$ erg/g/s)
$|\delta T/T|$
L(r)/L$_{tot}$
X$_C$
X$_H$
X$_{He}$
X$_i$ (mass fraction)
log q

Figure 2